Experimental evidence of orbital ferrimagnetism in $CoMnO_3$(0001) epitaxial thin film

Hiroki Koizumi,[1] Sonia Sharmin,[1] Kenta Amemiya,[2,3] Masako Suzuki-Sakamaki,[2,3,4] Jun-ichiro Inoue,[1] and Hideto Yanagihara[1,5]

[1]*Department of Applied Physics, University of Tsukuba, Tsukuba, Ibaraki 305-8573, Japan*
[2]*Institute of Materials Structure Science, High Energy Accelerator Research Organization, Tsukuba, Ibaraki 805-0801, Japan*
[3]*Department of Materials Structure Science, School of High Energy Accelerator Science, The Graduate University for Advanced Studies (SOKENDAI), Tsukuba, Ibaraki 305-0801, Japan*
[4]*Graduate School of Science and Technology, Gunma University, Kiryu, Gunma 376-8515, Japan*
[5]*Tsukuba Research Center for Energy Materials Science (TREMS), University of Tsukuba, Tsukuba, Ibaraki 305-8573, Japan*

(Received 4 December 2018; published 8 February 2019)

We have experimentally investigated the magnetic properties of $CoMnO_3$(0001) epitaxial films known to exhibit orbital ferrimagnetism. The films were grown by the reactive rf magnetron sputtering method. X-ray magnetic circular dichroism revealed that the spin momenta of Mn and Co ions are oriented opposite to each other and a large orbital momentum comparable to the spin angular momentum emerges only on Co, indicating the orbital ferrimagnetic nature of $CoMnO_3$. The magnetic anisotropy of $CoMnO_3$(0001) thin films was found to have a large negative value of $K_u = -15.6 \pm 0.8$ Merg/cm^3 at 300 K. The saturation magnetization was slightly smaller than the reported values of tiny single crystals, due to the presence of a sizable dead layer.

DOI: 10.1103/PhysRevMaterials.3.024404

I. INTRODUCTION

$CoMnO_3$ has an ilmenite structure ($R\bar{3}$) [1–4] in which Co^{2+} and Mn^{4+} layers are alternatively stacked along the c axis [3] (as shown in Fig. 1). Since Co^{2+} (d^7) and Mn^{4+} (d^3) possess $S = 3/2$, and are antiferromagnetically coupled through the superexchange interaction, the spin angular momenta of Co and Mn cancel each other out. However, the orbital angular momentum of Co^{2+} in the crystal field remains [3]. Since the experimentally estimated value of the magnetic moment is 0.72 μ_B/f.u. ($M_S = 140$ emu/cm^3 at 2 K), i.e., the same order of magnitude expected of the orbital angular momentum of Co^{2+} in an octahedral crystal field, this compound is termed an "orbital ferrimagnet."

Because of the remaining orbital angular momentum, $CoMnO_3$ possesses significantly large magnetic anisotropy. Cloud and Jesson succeeded in roughly estimating the magnetic anisotropy of $K_{u1} + 2K_{u2} \sim -14 \pm 2$ Merg/cm^3 through the extrapolation of the magnetization $M(H)$ curves taken up to 10 kOe for 60 miniature single crystals of $CoMnO_3$ [5]. They found that the c axis is a magnetically hard axis, indicating that $CoMnO_3$ has a negative magnetic anisotropy constant. Both the large orbital momentum and the large negative uniaxial anisotropy were partially explained within the framework of the single ion model of Co^{2+} [3], originally adapted for $CoFe_2O_4$ by Slonczewski [6,7]. Moreover, $CoMnO_3$ has a Néel temperature of 391 K [2]. Because of the unique origin of magnetism with a high transition temperature, $CoMnO_3$ is an attractive compound from the viewpoint of both fundamental magnetism and applications including novel devices for spintronics based on the orbital angular momentum [8–11]. However, previous experimental works regarding $CoMnO_3$ were mainly carried out on miniature single crystals, powder, or ceramic samples [1–3,12,13], not on sufficiently large single crystals or epitaxial films suitable for investigating the details of various properties. Therefore, the magnetic and other physical properties of $CoMnO_3$ are not well understood as yet.

In order to obtain direct experimental evidence of the nature of orbital ferrimagnetism in this compound, we grew epitaxial thin films of $CoMnO_3$(0001) on α-Al_2O_3(0001) by using the reactive radio-frequency (rf) magnetron sputtering technique [14–17], and carefully investigated the fundamental magnetic properties with a high field magnetization measurement and element selective x-ray magnetic circular dichroism measurements. This paper is organized as follows. The details of the experiments are explained in Sec. II. Section III is devoted to the experimental results and discussion, and the final section gives a summary of the work.

II. EXPERIMENT

$CoMnO_3$ thin films with thicknesses of 30, 33, 70, and 90 nm were grown by the reactive rf magnetron sputtering technique (ES-250MB: Eiko Engineering Co., Ltd.). We used a 2-in. alloy target with the desired composition of Co : Mn = 1 : 1. Prior to film growth, a single-crystal α-Al_2O_3(0001) substrate was ultrasonically degreased using acetone, ethanol, and de-ionized water for 5 min at each step. Afterward, the substrates were annealed at 1200 °C for 6 h in argon gas [19].

The growth conditions of $CoMnO_3$ thin films were as follows: O_2/Ar flow ratios were approximately 0.12, the process temperature was 770 °C, and the working pressure was 0.75 Pa. The film surface and the epitaxial growth were confirmed by the reflection high-energy electron diffraction (RHEED) technique. The film thicknesses were determined by x-ray reflectivity (XRR: Rigaku Smart Lab with Cu $K\alpha$ radiation). X-ray diffraction (XRD) analysis was performed

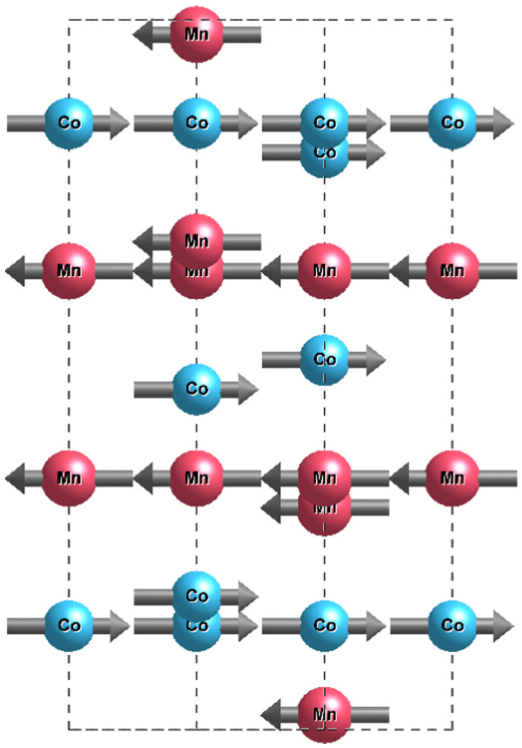

FIG. 1. Spin structure of $CoMnO_3$ drawn by VESTA [18].

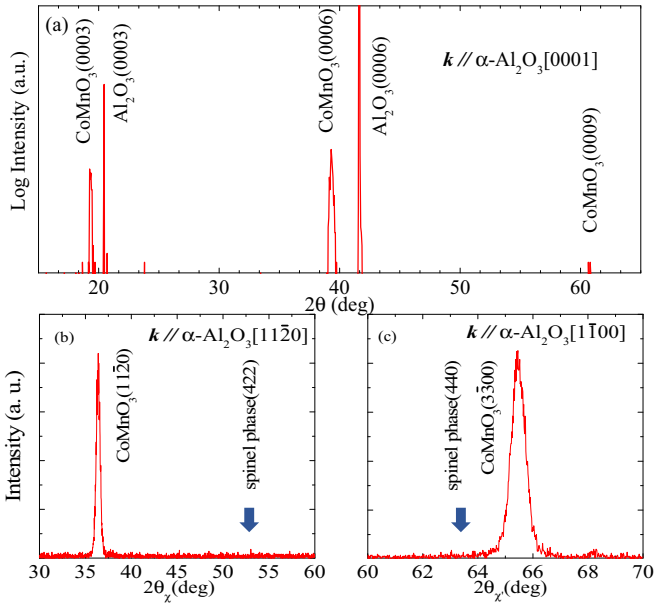

FIG. 2. (a)–(c) are the patterns of the scattering vector $\boldsymbol{k}$ parallel to [0001], [11$\bar{2}$0], and [1$\bar{1}$00], respectively.

to identify the crystal structure of the films. In-plane M-H loops and the magnetic anisotropy constant were respectively measured by a vibrating sample magnetometer (VSM) and a magnetotorque meter. Both measurements were performed by using the physical property measurement system (PPMS: Quantum Design). We applied fields up to 90 kOe at 300 K. The film composition was determined by the inductively coupled plasma mass-spectroscopy (ICP-MS) technique.

The valences of both Mn and Co ions were evaluated by the x-ray absorption near edge structure (XANES) experiment performed at BL-12C of KEK-PF. The XANES measurements were performed at room temperature. The photon energy was varied from 6502 to 6608 eV and 7674 to 7780 eV around the Mn and Co K edges, respectively. The incident angle of the x-rays was 45° with respect to the film. The x-ray absorption spectra (XAS) were obtained by the fluorescence method, which provides depth information to the degree of several tens of micrometers.

X-ray magnetic circular dichroism (XMCD) experiments were also performed at BL-16A of KEK-PF to evaluate the element specific spin angular and orbital angular momenta [20–22]. XMCD measurements for the film with a thickness of 70 nm were performed at room temperature. The photon energy was varied from 620 to 670 eV and 760 to 820 eV for the Mn and Co $L_{2,3}$ edges, respectively. The XAS were determined by the total electron yield (TEY) method. A set of XAS (μ_+ and μ_-) was measured using circularly polarized light with opposite helicity in a magnetic field of 50 kOe, applied parallel to the photon direction. The XMCD spectra were obtained by taking the difference of μ_+ and μ_-. The film plane was inclined 30° from both the incident photons and magnetic field so that the in-plane component of the magnetic moments could be detected. The degree of circular polarization was $\pm 95 \pm 4\%$ [23].

III. RESULTS AND DISCUSSION

A. Structural characterization

The XRD pattern of a 90-nm-thick $CoMnO_3$ film grown on a c-plane α-Al_2O_3 substrate is shown in Fig. 2. Figure 2(a) shows the XRD pattern with scattering vector $\boldsymbol{k}$ normal to the film and therefore parallel to α-Al_2O_3[0001]. Figures 2(b) and 2(c) show in-plane XRD patterns of the films along [11$\bar{2}$0] and [1$\bar{1}$00], respectively. All the observed Bragg peaks can be consistently assigned to a hexagonal structure. In Fig. 2(a), the diffraction peak corresponding to Al_2O_3(0003), which is a forbidden reflection, appears due to the effect of multiple diffraction of the α-Al_2O_3 substrate [24,25]. We note that there is no indication of the spinel phase of $(Co, Mn)_3O_4$ [26–28].

The determined epitaxial relationship between the film and substrate is $CoMnO_3(0001)[11\bar{2}0] \parallel \alpha\text{-}Al_2O_3(0001)[11\bar{2}0]$. Note that both (0003) and (0009) reflections can be seen in the XRD patterns. This indicates that the compound has an "ordered" structure, meaning that Co-ion and Mn-ion layers are stacked alternately along the c axis, and the grown film has an ilmenite crystal structure with space group of $R\bar{3}$ rather than the corundum of $R\bar{3}c$.

The composition ratio of the film was $Co : Mn = 0.46(\pm 0.02) : 0.54(\pm 0.03)$ as determined by ICP-MS. This suggests that the sputtering yield of Co is slightly less than that of Mn in alloy form during the reactive sputtering process.

B. Valence of cations

XANES spectra for the Mn and Co K edges are shown in Figs. 3(a) and 3(b), respectively. In Fig. 3(a), the two peaks are located approximately 2 eV apart. According to

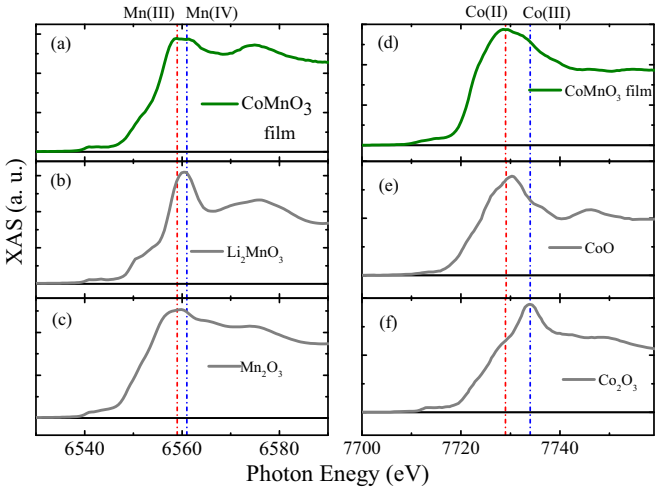

FIG. 3. Left: Mn K edge XANES spectra of (a) $CoMnO_3$ film, (b) Li_2MnO_3 [29], and (c) Mn_2O_3 [29]. Right: Co K edge XANES spectra of (d) $CoMnO_3$ film, (e) CoO [30], and (f) Co_2O_3 [30].

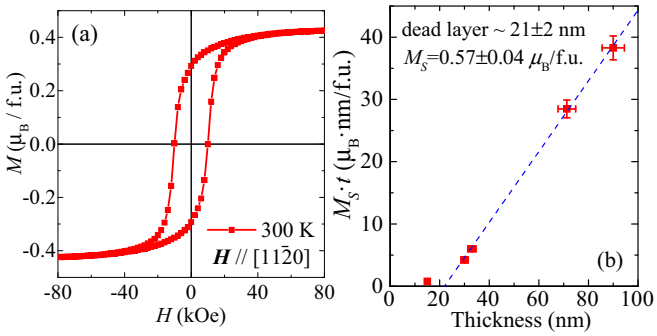

FIG. 4. (a) The in-plane M-H loop of 90-nm-thick $CoMnO_3(0001)$ films on the $Al_2O_3(0001)$ substrate at 300 K. (b) Plot of $M_S \cdot t$ as a function of thickness t. The x-axis intercept and the slope indicate the dead layer of 21 ± 2 nm and M_S of $0.57 \pm 0.04\,\mu_B$/f.u. (110 ± 7 emu/cm^3), respectively. The film thinner than the x-axis intercept is excluded when the fitting is performed.

the XANES spectra of Li_2MnO_3 [29], the peak position of Mn^{4+} in Li_2MnO_3 is located around 6561 eV, and that of Mn^{3+} in Mn_2O_3 [29] is located around 6559 eV. Since the two peak positions shown in Fig. 3(a) correspond to that of trivalent and quadrivalent Mn ions [29], our film contains both Mn^{3+} and Mn^{4+}. On the other hand, the strongest peak can be found at around 7729 eV in Fig. 3(b) corresponding to Co^{2+} [30], but very weak or no sign of Co^{3+} is observed at around 7734 eV [30].

As mentioned, the film was slightly Mn rich compared to stoichiometric $CoMnO_3$. Since the fundamental crystal structure is an ilmenite (ABO_3) and Co ions are mostly Co^{2+} ($S = 3/2$), the majority of the Mn ions are Mn^{4+} ($S = 3/2$). XANES results indicate that the main phase of the film is $Co^{2+}Mn^{4+}O_3{}^{2-}$ and the second phase may exist such as $Mn_2{}^{3+}O_3{}^{2-}$.

C. Magnetic properties

In order to measure magnetization, the magnetic field was applied along the in-plane direction. Figure 4(a) shows an M-H loop at 300 K with 90-nm-thick $CoMnO_3(0001)$ films grown on the α-$Al_2O_3(0001)$ substrate. A saturation magnetization of $M_S = 0.42\,\mu_B$/f.u. (81 emu/cm^3) is obviously less than the reported value of $M_S = 0.61\,\mu_B$/f.u. (120 emu/cm^3) for the ceramic sample at room temperature [3], implying the existence of a magnetic dead layer.

In order to evaluate the dead layer of the $CoMnO_3$ films, we plot the areal saturation magnetization $M_S \cdot t$ as a function of thickness (t), shown in Fig. 4(b). All the data points thicker than 30 nm seem to be on a single straight line. We fitted the data points to estimate both the dead-layer thickness and the intrinsic M_S of the $CoMnO_3$ film. The obtained dead-layer thickness and M_S are 21 ± 2 nm and $0.57 \pm 0.04\,\mu_B$/f.u. (110 ± 7 emu/cm^3), respectively. In fact, the film of 15-nm thickness which is thinner than the x-axis intercept in Fig. 4(b) has almost no magnetization. By taking account of the existence of the dead layer, the *intrinsic* M_S of 110 ± 7 emu/cm^3 at room temperature is almost the same as the reported value for the bulk sample [3]. Since $CoMnO_3$ is a layered compound, the initial growth of the film may not be ordering. Moreover, some defects, such as antiphase boundaries and stacking faults, shift along the ordered c axis, which may be the origin of the dead layer.

The magnetotorque curve of the $CoMnO_3$ thin film at 90 kOe with a film thickness of 90 nm is shown in Fig. 5. The measurements were performed at 300 K. The torque curve indicates that the magnetic easy axis lies in plane. Even at 90 kOe, the torque curve exhibits a sawtooth-wave-like shape with clear rotational hysteresis, indicating that the anisotropy field is significantly greater than 90 kOe.

The uniaxial magnetic anisotropy energy can be written as $E = K_u^{\text{eff}} \sin^2\theta$, where K_u^{eff} and θ are the effective uniaxial magnetic anisotropy constant and the angle between magnetization $\boldsymbol{M}$ and the normal to the film, respectively. The observed K_u^{eff} comprises both magnetic anisotropy contributions from magnetocrystalline anisotropy K_u and shape anisotropy $2\pi M_S^2$, i.e., $K_u^{\text{eff}} = K_u - 2\pi M_s^2$. Hereafter, we exclude the dead layer to evaluate the volume and K_u as well.

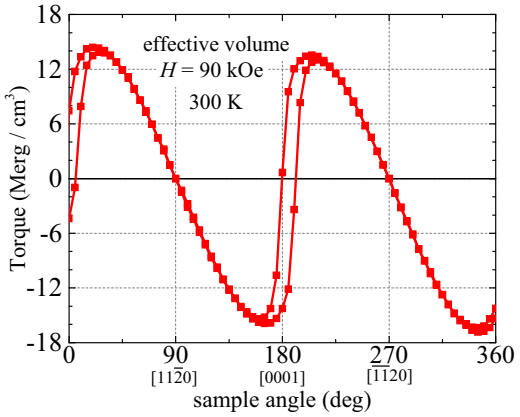

FIG. 5. Magnetotorque curve of a $CoMnO_3$ thin film with a film effective thickness of 69 nm, and a nominal thickness of 90 nm at 90 kOe.

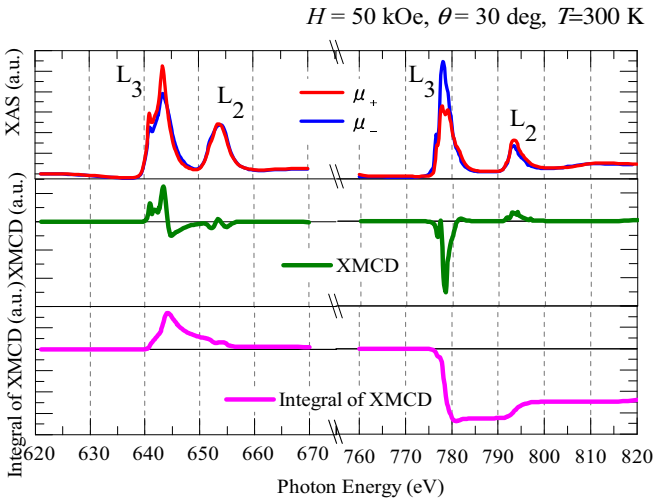

FIG. 6. Mn and Co circularly polarized XAS (μ^+ and μ^-), XMCD spectra ($\mu^+ - \mu^-$), and the integral of XMCD spectra.

$K_u^{\rm eff}$ determined from peak to peak of the torque curve is -15.6 ± 0.8 Merg/cm^3, meaning the anisotropy field $H_k = 2|K_u|/M_S = 283$ kOe. Note that $2\pi M_S^2$ is 6.3×10^4 erg/cm^3, which is negligibly smaller than the value of K_u. Therefore the intrinsic $K_u \approx K_u^{\rm eff}$ of the $CoMnO_3$ thin film is found to be -15.6 ± 0.8 Merg/cm^3 at 300 K, which is almost the same as the previously reported value of $K_u = -14 \pm 2$ Merg/cm^3 at room temperature [5].

D. XMCD analysis

Figure 6 shows Mn $2p$ XAS and XMCD spectra as well as those of Co $2p$ observed for the $CoMnO_3$ film. We applied the XMCD sum rules [31–33] to the spectra in order to estimate the ratio of orbital to spin magnetic moment $m_{\rm orb}/m_{\rm spin}$, which can be expressed as

$$\frac{m_{\rm orb}}{m_{\rm spin} + 7\langle T_Z\rangle} = \frac{2}{3}\frac{\int_{L_{2,3}}(\mu_+ - \mu_-)d\omega}{\int_{L_3}(\mu_+ - \mu_-)d\omega - 2\int_{L_{2,3}}(\mu_+ - \mu_-)d\omega}. \quad (1)$$

In addition, the projection components of spin and orbital moments along the magnetic field direction are respectively expressed as follows,

$$m_{\rm spin} = n_h \frac{3\int_{L_3} d\omega(\mu_+ - \mu_-) - 2\int_{L_3+L_2} d\omega(\mu_+ - \mu_-)}{\int_{L_3+L_2} \frac{1}{2}(\mu_+ + \mu_-)\left\{1 + \frac{7\langle T_z\rangle}{2\langle S_z\rangle}\right\}}, \quad (2)$$

$$m_{\rm orb} = n_h \frac{2}{3}\frac{\int_{L_3+L_2} d\omega(\mu_+ - \mu_-)}{\int_{L_3+L_2} d\omega\frac{1}{2}(\mu_+ + \mu_-)}. \quad (3)$$

Here, $\langle T_Z\rangle$ in Eqs. (1) and (2) is an expectation value of the magnetic dipole operator. $\langle T_Z\rangle$ is supposed to be zero when the film plane is aligned to be 35.3° off, known as the magic angle [34]. Hereafter, we assume that $\langle T_Z\rangle$ is negligible because our experimental setup of degrees was sufficiently close to the magic angle. Therefore, the left-hand side of Eq. (1) can be written as $m_{\rm orb}/m_{\rm spin}$.

From the XMCD spectra shown in Fig. 6, the $m_{\rm orb}/m_{\rm spin}$ ratios evaluated with Eq. (1) are determined to be 0.022 ± 0.002 for Mn and 0.33 ± 0.03 for Co, respectively. It is obvious that the larger contribution of the orbital moment comparable to the spin angular moment was found only for Co. In addition, by comparing the shapes of the XMCD spectra for Co and Mn, we can conclude that the magnetic moments of Mn and Co are oriented in opposite directions. Note that Eq. (1) requires no information on the average number of $3d$ holes $n_h = 10 - n_{3d}$ with the number of $3d$ electrons of n_{3d}, nor the degree of circular polarization of the incident photons.

Next, we evaluated both spin and orbital moments for Mn and Co by applying Eqs. (2) and (3). From Eq. (2), $m_{\rm spin}$'s for Mn and Co are evaluated as $1.2 \pm 0.2\,\mu_B$ and $0.9 \pm 0.2\mu_B$, respectively. Here, we assumed that n_{3d}'s of Mn^{4+} [35] and Co^{2+} [36] are 3.8 and 7.21, respectively. Both $m_{\rm spin}$'s are the same within the experimental error. On the other hand, $m_{\rm orb}$'s are estimated by Eq. (3) to be $0.02 \pm 0.00\,\mu_B$ for Mn^{4+} and $0.31 \pm 0.06\,\mu_B$ for Co^{2+}. Assuming that the spin components are totally canceled out and therefore the observed magnetization is simply originated from the orbital moment of Co, $m_{\rm orb}$ of Co^{2+} seems to be clearly smaller than $M_s = 0.57 \pm 0.04\,\mu_B$/f.u. from the magnetization measurement shown in Fig. 4. The discrepancy is probably due to the the difference in the measurement geometries between the in-plane magnetization measurement and the XMCD experiment with the oblique incident beam. Since the anisotropic magnetic field is as high as 280 kOe, M is neither oriented along the direction of the external magnetic field nor saturated at 50 kOe in our XMCD experiment.

The L_3 edge corresponds to excitation from the $2p$ to $3d$ core state, so we can also determine the valences from XAS and XMCD. XAS and XMCD spectra around the Mn L_3 edge have double peaks as shown in Fig. 6. This is a similar structure observed in Mn^{4+} of La_2MnCoO_6 [37]. If Mn^{3+} is dominant, the L_3 edge shows a single peak in both XAS and XMCD as observed in $LaMnO_3$ [37]. In other words, it can also be known from XAS and XMCD that the $CoMnO_3$ thin film mainly consists of Mn^{4+}. In the case of Co, XMCD spectra are almost the same as those of Co^{2+} of La_2MnCoO_6 [37], meaning the $CoMnO_3$ thin film is composed of Co^{2+}. The spectra are totally different from the L_3 edge of Co^{3+} having a single peak observed in $LaCoO_3$ [38]. The fact that the observed Mn state is quadrivalent does not seem to be consistent with the XANES results. The discrepancy could be explained by the difference in the probing depth of the two techniques. The probing depth in the TEY method is $\leqslant$5 nm [39], whereas that of the fluorescence method with a hard x-ray is typically several tens of micrometers. Therefore, it is expected that the Mn^{3+} exists far from the surface, suggesting that the dead layer is present at the vicinity of interface but not at the surface.

IV. CONCLUSION

In this study, we succeeded in growing epitaxial $CoMnO_3(0001)$ thin films on α-Al_2O_3 by the rf magnetron

sputtering method with oxygen gas. The thickness-dependent magnetization revealed the existence of a magnetic dead layer with a thickness of around 21 ± 2 nm. The magnetic anisotropy of the $CoMnO_3$ thin film is negative, and the value of K_u is -15.6 ± 0.8 Merg/cm^3, as estimated by the magnetotorque experiment. XANES and XMCD results consistently explained the presence of orbital ferrimagnetism in that the magnetic properties are predominantly determined by the remaining orbital angular momentum of Co^{2+} and the spin angular momenta of both Mn^{4+} and Co^{2+} are canceled. In the future, considering the application to spintronics devices, it is necessary to suppress the dead layer, meaning the development of appropriately improving the buffer layer should be addressed.

ACKNOWLEDGMENTS

This work was performed under the approval of the Photon Factory Program Advisory Committee (Proposals No. 2017G602 and No. 2016S2-005). H.K. thanks M. Mizumaki and M. Kitamura for their valuable comments.

[1] W. H. Cloud, Crystal structure and ferrimagnetism in $NiMnO_3$, and $CoMnO_3$, Phys. Rev. **111**, 1046 (1958).
[2] T. J. Swoboda, R. C. Toole, and J. D. Vaughan, New magnetic compounds of the ilmenite type structure, J. Phys. Chem. Solids **5**, 293 (1958).
[3] R. M. Bozorth and D. E. Walsh, Ferromagnetic moment of $CoMnO_3$, J. Phys. Chem. Solids **5**, 299 (1958).
[4] W. P. Wolf, Ferrimagnetism, Rep. Prog. Phys. **24**, 212 (1961).
[5] W. H. Cloud and J. P. Jesson, Magnetic anisotropy in $CoMnO_3$, J. Appl. Phys. **37**, 1398 (1966).
[6] J. C. Slonczewski, Origin of magnetic anisotropy in cobalt-substituted magnetite, Phys. Rev. **110**, 1341 (1958).
[7] M. Tachiki, Origin of the magnetic anisotropy energy of cobalt ferrite, Prog. Theor. Phys. **23**, 1055 (1960).
[8] A. Manchon, H. C. Koo, J. Nitta, S. M. Frolov, and R. A. Duine, New perspectives for Rashba spin-orbit coupling, Nat. Mater. **14**, 871 (2015).
[9] K.-U. Demasius, T. Phung, W. Zhang, B. P. Hughes, S.-H. Yang, A. Kellock, W. Han, A. Pushp, and S. S. P. Parkin, Enhanced spin-orbit torques by oxygen incorporation in tungsten films, Nat. Commun. **7**, 10644 (2016).
[10] S. D. Stranks and P. Plochocka, The influence of the Rashba effect, Nat. Mater. **17**, 381 (2018).
[11] X. Chen, Y. Liu, G. Yang, H. Shi, C. Hu, M. Li, and H. Zeng, Giant antidamping orbital torque originating from the orbital Rashba-Edelstein effect in ferromagnetic heterostructures, Nat. Commun. **9**, 2569 (2018).
[12] A. Petric and H. Ling, Electrical conductivity and thermal expansion of spinels at elevated temperatures, J. Am. Ceram. Soc. **90**, 1515 (2007).
[13] I. O. Troyanchuk, A. A. Shemyakov, and V. K. Prokopenko, Magnetic structure of $NiMnO_3$ and $CoMnO_3$ ilmenites, Phys. Status Solidi A **113**, K107 (1989).
[14] T. Niizeki, Y. Utsumi, R. Aoyama, H. Yanagihara, J.-i. Inoue, Y. Yamasaki, H. Nakao, K. Koike, and E. Kita, Extraordinarily large perpendicular magnetic anisotropy in epitaxially strained cobalt-ferrite $Co_xFe_{3-x}O_4(001)$ ($x = 0.75, 1.0$) thin films, Appl. Phys. Lett. **103**, 162407 (2013).
[15] H. Yanagihara, M. Myoka, D. Isaka, T. Niizeki, K. Mibu, and E. Kita, Selective growth of Fe_3O_4 and α-Fe_2O_3 films with reactive magnetron sputtering, J. Phys. D: Appl. Phys. **46**, 175004 (2013).
[16] T. Ojima, T. Tainosho, S. Sharmin, and H. Yanagihara, RHEED oscillations in spinel ferrite epitaxial films grown by conventional planar magnetron sputtering, AIP Adv. **8**, 045106 (2018).
[17] H. Onoda, H. Sukegawa, E. Kita, and H. Yanagihara, Control of magnetic anisotropy by lattice distortion in cobalt ferrite thin film, IEEE Trans. Magn. **54**, 1 (2018).
[18] K. Momma and F. Izumi, VESTA 3 for three-dimensional visualization of crystal, volumetric and morphology data, J. Appl. Crystallogr. **44**, 1272 (2011).
[19] B. Qi, B. Agnarsson, K. Jonsson, S. Olafsson, and H. P. Gislason, Characterisation of high-temperature annealing effects on α-Al_2O_3 (0001) substrates, J. Phys.: Conf. Ser. **100**, 042020 (2008).
[20] K. Amemiya, A. Toyoshima, T. Kikuchi, T. Kosuge, K. Nigorikawa, R. Sumii, and K. Ito, Commissioning of a soft x-ray beamline PF-BL-16A with a variable-included-angle varied-line-spacing grating monochromator, in *SRI 2009, 10th International Conference on Radiation Instrumentation*, edited by R. Garrett, I. Gentle, K. Nugent, and S. Wilkins, AIP Conf. Proc. Vol. 1234 (AIP, Melville, NY, 2010), p. 295.
[21] K. Ikeda, T. Seki, G. Shibata, T. Kadono, K. Ishigami, Y. Takahashi, M. Horio, S. Sakamoto, Y. Nonaka, M. Sakamaki, K. Amemiya, N. Kawamura, M. Suzuki, K. Takanashi, and A. Fujimori, Magnetic anisotropy of l10-ordered FePt thin films studied by Fe and Pt $L_{2,3}$-edges x-ray magnetic circular dichroism, Appl. Phys. Lett. **111**, 142402 (2017).
[22] S. Sakamoto, K. Srinivasan, R. Zhang, O. Krupin, K. Ikeda, G. Shibata, Y. Nonaka, Z. Chi, M. Sakamaki, K. Amemiya, A. Fujimori, and A. Ajan, Effects of cobalt substitution in $L1_0$-(Fe,Co)Pt thin films, Phys. Rev. B **96**, 144437 (2017).
[23] D. Asakura, T. Koide, S. Yamamoto, K. Tsuchiya, T. Shioya, and K. Amemiya, Magnetic states of Mn and Co atoms at Co_2MnGe/MgO interfaces seen via soft x-ray magnetic circular dichroism, Phys. Rev. B **82**, 184419 (2010).
[24] M. Renninger, "Umweganregung," eine bisher unbeachtete Wechselwirkungserscheinung bei Raumgitterinterferenzen, Z. Phys. **106**, 141 (1937).
[25] P. Zaumseil, High-resolution characterization of the forbidden Si 200 and Si 222 reflections, J. Appl. Crystallogr. **48**, 528 (2015).
[26] N. Garg, M. Mishra, G. Govind, and A. Kumar Ganguli, Electrochemical and magnetic properties of nanostructured $CoMn_2O_4$ and Co_2MnO_4, RSC Adv. **5**, 84988 (2015).
[27] K. Uusi-Esko, E.-L. Rautama, M. Laitinen, T. Sajavaara, and M. Karppinen, Control of oxygen nonstoichiometry and magnetic property of $MnCo_2O_4$ thin films grown by atomic layer deposition, Chem. Mater. **22**, 6297 (2010).

[28] E. Ríos, O. Peña, T. Guizouarn, and J.-L. Gautier, Thin films of Co_3O_4, $MnCo_2O_4$ and their solid solution as electrocatalyst: Study of their magnetic properties, Phys. Status Solidi C **1**, S108 (2004).

[29] C. S. Johnson, J. S. Kim, A. J. Kropf, A. J. Kahaian, J. T. Vaughey, L. M. L. Fransson, K. Edström, and M. M. Thackeray, Structural characterization of layered $Li_xNi_{0.5}Mn_{0.5}O_2$ ($0 < x \leqslant 2$) oxide electrodes for Li batteries, Chem. Mater. **15**, 2313 (2003).

[30] Y. Takahash, A. Usui, K. Okumura, T. Uruga, M. Nomura, M. Murakami, and H. Shimizu, Application of XANES for the determination of oxidation states of Co and Pb in natural ferromanganese nodules, Chem. Lett. **31**, 366 (2002).

[31] B. T. Thole, P. Carra, F. Sette, and G. van der Laan, X-Ray Circular Dichroism as a Probe of Orbital Magnetization, Phys. Rev. Lett. **68**, 1943 (1992).

[32] P. Carra, B. T. Thole, M. Altarelli, and X. Wang, X-Ray Circular Dichroism and Local Magnetic Fields, Phys. Rev. Lett. **70**, 694 (1993).

[33] J. Stöhr and H. König, Determination of Spin- and Orbital-Moment Anisotropies in Transition Metals by Angle-Dependent X-Ray Magnetic Circular Dichroism, Phys. Rev. Lett. **75**, 3748 (1995).

[34] T. Koide, H. Miyauchi, J. Okamoto, T. Shidara, A. Fujimori, H. Fukutani, K. Amemiya, H. Takeshita, S. Yuasa, T. Katayama, and Y. Suzuki, Direct Determination of Interfacial Magnetic Moments with a Magnetic Phase Transition in Co Nanoclusters on Au(111), Phys. Rev. Lett. **87**, 257201 (2001).

[35] T. Saitoh, A. E. Bocquet, T. Mizokawa, H. Namatame, A. Fujimori, M. Abbate, Y. Takeda, and M. Takano, Electronic structure of $La_{1-x}Sr_xMnO_3$ studied by photoemission and x-ray-absorption spectroscopy, Phys. Rev. B **51**, 13942 (1995).

[36] G. van der Laan, E. Arenholz, R. V. Chopdekar, and Y. Suzuki, Influence of crystal field on anisotropic x-ray magnetic linear dichroism at the $Co^{2+}L_{2,3}$ edges, Phys. Rev. B **77**, 064407 (2008).

[37] K. Yoshimatsu, H. Wadati, E. Sakai, T. Harada, Y. Takahashi, T. Harano, G. Shibata, K. Ishigami, T. Kadono, T. Koide, T. Sugiyama, E. Ikenaga, H. Kumigashira, M. Lippmaa, M. Oshima, and A. Fujimori, Spectroscopic studies on the electronic and magnetic states of Co-doped perovskite manganite $Pr_{0.8}Ca_{0.2}Mn_{1-y}Co_yO_3$ thin films, Phys. Rev. B **88**, 174423 (2013).

[38] T. Burnus, Z. Hu, H. H. Hsieh, V. L. J. Joly, P. A. Joy, M. W. Haverkort, H. Wu, A. Tanaka, H. Lin, C. T. Chen, and L. H. Tjeng, Local electronic structure and magnetic properties of $LaMn_{0.5}Co_{0.5}O_3$ studied by x-ray absorption and magnetic circular dichroism spectroscopy, Phys. Rev. B **77**, 125124 (2008).

[39] R. Nakajima, J. Stöhr, and Y. Idzerda, Electron-yield saturation effects in *L*-edge x-ray magnetic circular dichroism spectra of Fe, Co, and Ni, Phys. Rev. B **59**, 6421 (1999).